The 8th European Congress on Computational Methods in Applied Sciences and Engineering
ECCOMAS Congress 2022
5 – 9 June 2022, Oslo, Norway

A MIXED FIDELITY CONCEPTUAL DESIGN PROCESS FOR BOUNDARY LAYER INGESTION CONCEPTS ECCOMAS CONGRESS 2022

O. ATINAULT [*], M. MEHEUT[*] AND S. DEFOORT[†]

[*] ONERA, Université Paris-Saclay, Meudon, France
† ONERA, Université de Toulouse, Toulouse, France
e-mail: olivier.atinault@onera.fr, michael.meheut@onera.fr, sebastien.defoort@onera.fr
www.onera.fr

Key words: Aerodynamics, Propulsion, Computing Methods, Boundary Layer Ingestion, BLI

Abstract. Boundary Layer Ingestion (BLI) is a promising concept that helps improving aircraft aeropropulsive performance. However, it remains difficult to bring together OAD (Overall Aircraft Design) process and high-fidelity tools due to the time of response of complex disciplinary tools. ONERA has thus developed a mixed fidelity approach inside its in-house OAD platform. The purpose is to mix conventional and robust OAD methods with high levels of fidelity from disciplinary tools such as CFD (Computational Fluid Dynamics), FEM (Finite Element Model) or CAA (Computational Aero Acoustics). This paper focuses on the integration of rapid CFD tools inside the OAD process, in order to assess BLI benefits.

The resulting process is validated against reference and experimental cases when available, or high-fidelity RANS data elsewhere. The paper intends to present the tools and their validation process. These modules are applied to the common inlet concept, which aims at ingesting 100% of the fuselage boundary layer. The results demonstrate the potential gain on the Power Saving Coefficient (up to 3% obtained with the L2 BLI module without resizing loop) but with non-negligible fan losses (up to 1.5%).

1 INTRODUCTION

Boundary Layer Ingestion is one amongst promising concepts that would help improving aircraft aeropropulsive performance. Several studies ([1]to[12]) have already highlighted the benefit of that technology, either at OAD (Overall Aircraft Design) level with low fidelity models ([1], [5], [9], [10]) or in CFD (Computational Fluid Dynamics) studies with high-fidelity tools on particular cases ([2], [3], [7], [8], [11], [12]). However, exploring the design space of such technology and its integration onto an aircraft concept is still a challenge, as it remains difficult to bring together OAD and high-fidelity tools due to the time of response of complex disciplinary tools. Within the European Clean Sky 2 AIRFRAME ITD platform ONERA has thus developed a mixed fidelity approach inside its in-house OAD platform. The purpose is to mix various levels of fidelity from disciplinary tools (CFD, FEM, CAA), with the conventional and robust OAD methods. This paper focuses on the integration of rapid

CFD tools inside the OAD process, in order to assess BLI benefits.

The purpose of ONERA's OAD platform, named MYSTIC [16], is to provide a software environment in which main aircraft disciplines can contribute, and be able to capture the interaction effects between them and the corresponding snowball effects in the aircraft figures of merit such as fuel burn, mass breakdown or aero-propulsive efficiency. Each major discipline can be integrated through a dedicated expert tool, to improve the accuracy of the aircraft performance prediction at OAD level. Depending on their level of fidelity to the physics, tools are classified as Level 0 (values from charts, abacus, semi-empirical formulae), Level 1 (basic physical equations are solved), and Level 2 (advanced physical equations are solved, using expert software such as CFD tools or FEM for example). The time of response must remain acceptable with respect to the OAD process, which may require several sizing loops or optimization with respect to specific parameters.

As far as BLI is concerned, its integration within MYSTIC relies on those three fidelity levels (Figure 4). Level 0 is modelled by using a BLI effect proportional to the quantity of ingested drag, and is based on [13]. Level 1 is using a model of boundary layer growth using a simple integral method. A power law provides then the boundary layer profiles, which are finally sent to a Power Balance method [14]. Level 2 is of much higher fidelity: the geometry of the aircraft shape is generated by MYSTIC, then meshed and computed using a CFD Euler code. The pressure field on the fuselage is then recovered, and a boundary layer code, accounting for adverse pressure gradients, provides a boundary layer shape. That result is then used to assess the BLI performance more accurately with the Power Balance method [14]. It is also used to estimate the flow field in the fan plane, which is sent to a Parallel Compressor Method [15] in order to estimate the fan efficiency losses. More details are given in §3.

In the paper, a brief overview of the OAD ONERA MYSTIC process as well as a description of the CANOE aerodynamic module is given in §2. §3 provides details about the L0, L1 and L2 BLI modules and their validation in different aerodynamic conditions. The last section is dedicated to this application on the method on the Common Inlet BLI concept.

2 MYSTIC OAD PROCESS

2.1 MYSTIC:

Integrated OAD activities have been running at ONERA for a long time, but the existing tool suites were either based on commercial integration softwares, or not sufficiently modular to perform MDO (Multi-Disciplinary Optimization) studies. Therefore a large effort was undertaken to define a new, modular, evolutive tool to conduct the configuration studies, first at L0 level. The enhanced version calibrated and improved with ONERA internal knowledge has then been developed under the name of MYSTIC, and will be used in this study.

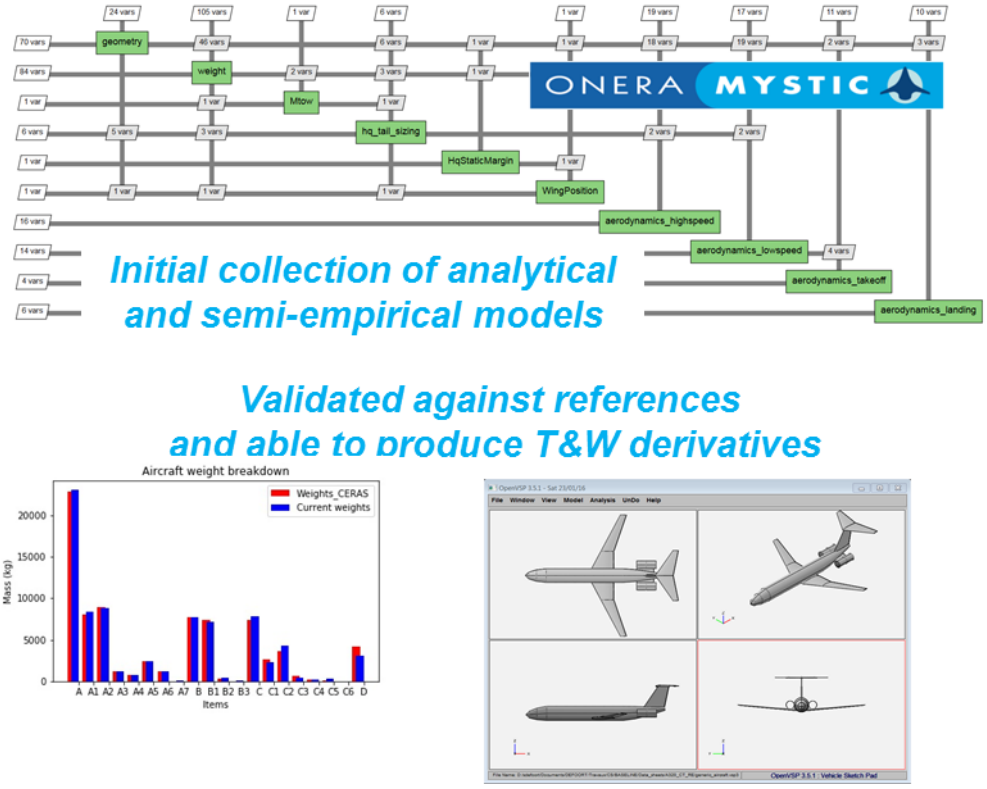

Figure 1: inputs and outputs of the MYSTIC tool.

This tool incorporates physical modules for the classical disciplines of Overall Aircraft Design: Propulsion, Aerodynamics, Mass breakdown and balance, Handling qualities, Trajectory and Performance. Three sizing loops are implemented, allowing designing an aircraft upon its TLARs with iterations on the disciplinary modules:

- Loop 1: design of HTP and VTP surfaces upon trimmability and stability HQ criterions at take-off and in cruise, iterating on the CoG position,
- Loop 2: iteration on the wing position to ensure a desired static margin, after calculation of aerodynamic center,
- Loop 3: iteration on the maximum take-off weight (updated after OWE and mission fuel calculation) and wing size (to ensure required approach speed and accommodate the mission fuel).

The baseline version of MYSTIC incorporates mostly L0 methods, which enable quick sizing and computation of sensitivities on conventional aircraft (tube and wing architecture). Underlying disciplinary methods can be described as follows:

- Geometry
  - Fuselage dimensions computed with respect to cabin layout
  - Parametric geometry of lifting surfaces
- Aerodynamics
  - Friction drag estimated through wetted area and cf(Reynolds) correlations
  - Induced drag estimated through Oswald coefficient (function of Mach)
  - Low-speed CL and CD computed by XFOIL (clean) and through Raymer-type correlations (flapped)
- Mass breakdown
  - Simplified loads : gust at maximum and minimum weights
  - Collection of parametric empirical correlations for each structural component and systems, enabling a detailed estimation of OWE
- Propulsion
  - Definition of a « rubber » engine scalable with respect to SLS thrust, BPR, OPR,…
- Mission/Trajectory
  - Full timestep integration of all the mission phases
  - Constant altitude, continuous climb options (soon step climb)
  - Can be replaced by Breguet range equation

This baseline version of MYSTIC and the corresponding L0 modules, jointly developed with ISAE-SUPAERO, have been wrapped into the NASA OpenMDAO framework and made publicly available under the name of FAST-OAD [29].

The logic of the on-going ONERA aircraft design studies is to progressively replace the L0 tools pre-existing in MYSTIC by the higher fidelity modules, such as the BLI module. In order to achieve this goal, a common input/output XML file is used, gathering the whole description of the aircraft through a dictionary of parameters. The geometrical parameterization is shared among all the modules and enables to generate an OpenVSP [19] CAD model for visualization and disciplinary computation purposes.

2.2 CANOE

This CANOE module [16] is based on Euler-CFD computations performed by the *SU²* [17] or elsA (Airbus-Safran-ONERA property) codes and on the in-house ONERA far-field drag decomposition tools *ffd* [18]. This tool enables, from a CFD solution, to compute the different physical drag components (viscous, wave and induced) and eliminate the non-physical drag sources, called spurious drag. Thanks to this approach, the sensitivity of the total drag with respect to the mesh is drastically reduced compared to classical near-field integration methods. This aerodynamic module also provides the other aerodynamic coefficients (notably the lift and pitching moment coefficients). The surface meshes used for the Euler

computations are created using *OpenVSP* [19] and the geometry defined by MYSTIC. The unstructured final volume meshes are generated using *tetgen* [27].

To ensure an accurate and reliable evaluation of the total drag during the optimization process at OAD level, a detailed parametric study with respect to mesh parameters has been achieved and coupled with the post-processing procedure using *ffd*.

To validate the cruise aerodynamic performance, a simplified configuration based of the CeRas configuration was defined ([28]). This configuration is composed on a single trapezoidal wing (without kink) and fuselage. In order to evaluate the impact of the Aspect Ratio (AR) on the aerodynamic performance, several configurations with different ARs ranging from 6 to 20 were designed, keeping all other wing parameters constant (wing area, sweep angle, taper ratio, thickness and twist spanwise distributions) to obtain as much as possible a pure AR effect. The results are depicted in Figure 2 and Figure 3 for C_L=0.6. Figure 2 shows the influence of the Aspect Ratio on the wing pressure distributions and Figure 3 on the induced and wave drag components.

Figure 2 highlights the wingspan increase with the AR as well as the decrease of the Mean Aerodynamic Chord (constant wing area). As expected for all configurations, the flow topology on the upper part of the wing remains identical (scaling effect) and the intensity of the shock wave consistent.

The evolutions of the induced and wave drag components with respect to the Aspect Ratio are shown in Figure 3 for C_L=0.6. For the induced drag, the results are compared to the theoretical minimum induced drag values obtained for an elliptic wing distribution. For both components, the two curves correspond respectively to the results obtained without and with aircraft sizing (see details in [16]) in the MYSTIC process. This means that for the sizing case, the wing area slightly evolves with the AR depending on the mass equilibrium. Consequently, the results in Figure 3 show that the impact of the sizing is relatively small but enable to demonstrate that:

- the aerodynamic module provides results consistent with the theory (constant wave drag and decrease of the induced drag similar to the theoretical minimum induced drag);
- the correct integration of the aerodynamic module in the OAD process.

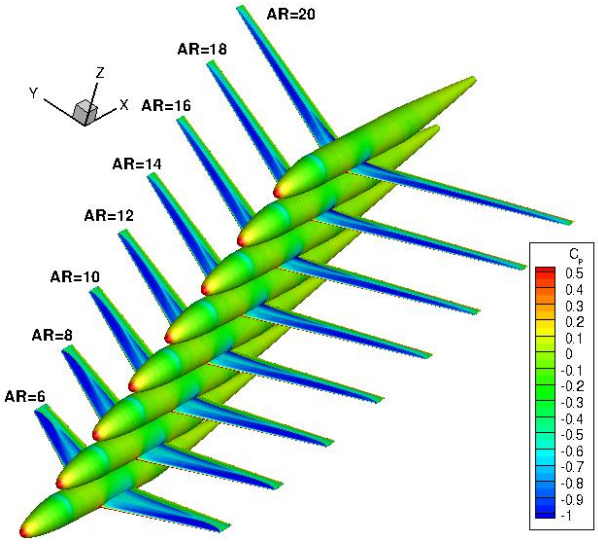

Figure 2: Aerodynamic module - Influence of Aspect Ratio on the surface pressure distribution.

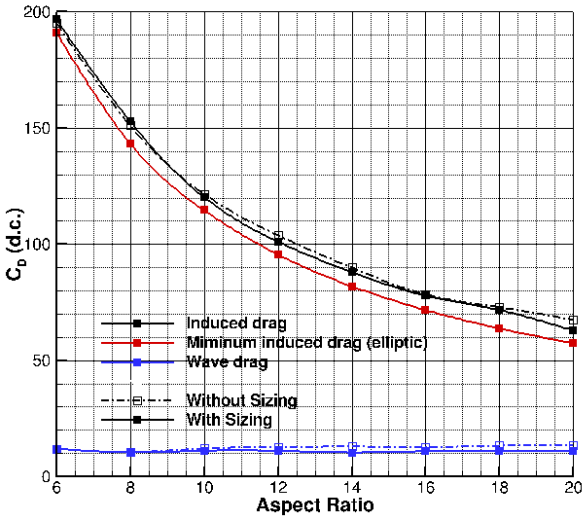

Figure 3: Aerodynamic module - Influence of Aspect Ratio on the drag coefficient (induced and wave components).

3 ADDING BLI FUNCTIONNALITIES TO MYSTIC

The modular framework of MYSTIC allows an easy insertion of multidisciplinary modules. The BLI modules are standalone Python routines that are called by the main MYSTIC process. Depending on the level of accuracy required for BLI estimation, more or less inputs are extracted from the dictionary of MYSTIC (such as flight conditions, engine sizing or geometrical dimensions). Three levels of fidelity are implemented into MYSTIC (Figure 4).

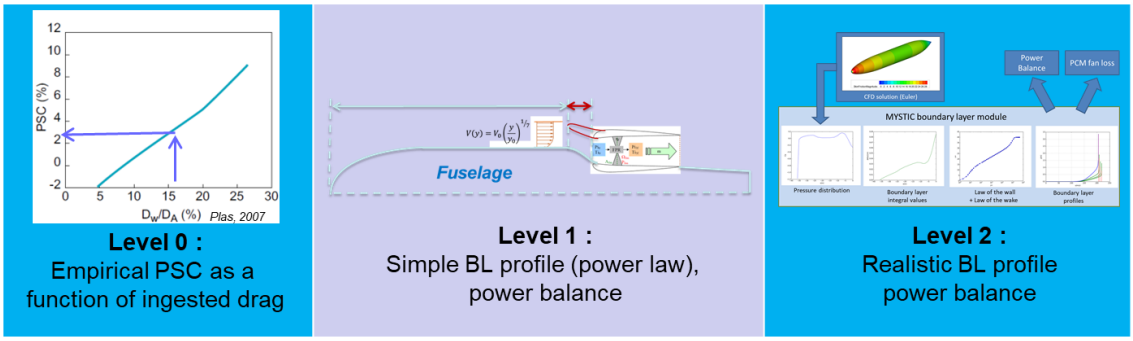

Figure 4: BLI modules - The three fidelity levels for BLI modeling in the OAD tool MYSTIC.

All processes allow to compute the Power Saving Coefficient “PSC” (equation (1) from [1]), which is based on the estimation of the reduction of the propulsive power required to sustain the flight at constant speed and altitude.

$$\mathrm{PSC}(\%) = \frac{\mathrm{Power}_{\mathrm{noBLI}} - \mathrm{Power}_{\mathrm{BLI}}}{Power_{\mathrm{noBLI}}} \quad (1)$$

3.1 Level 0 BLI process

BLI Level 0 is modelled by using a BLI effect proportional to the quantity of ingested drag, and is based on [13].

Assuming that the BLI benefit is directly proportional to the quantity of aircraft drag that is ingested by the engines, the computation of the BLI gain is purely geometrical. Before coming into the inlet of the engine, the air travels along a portion of the fuselage skin (whether it is a cylinder or a blended wing body). This "ingested surface" can be estimated by knowing the intersection between the engine and the airframe, as illustrated in Figure 5. Considering that most of the fuselage drag is composed of friction drag, the knowledge of that "ingested surface" provides the quantity of ingested drag with a simple correlation (see Figure 5 left).

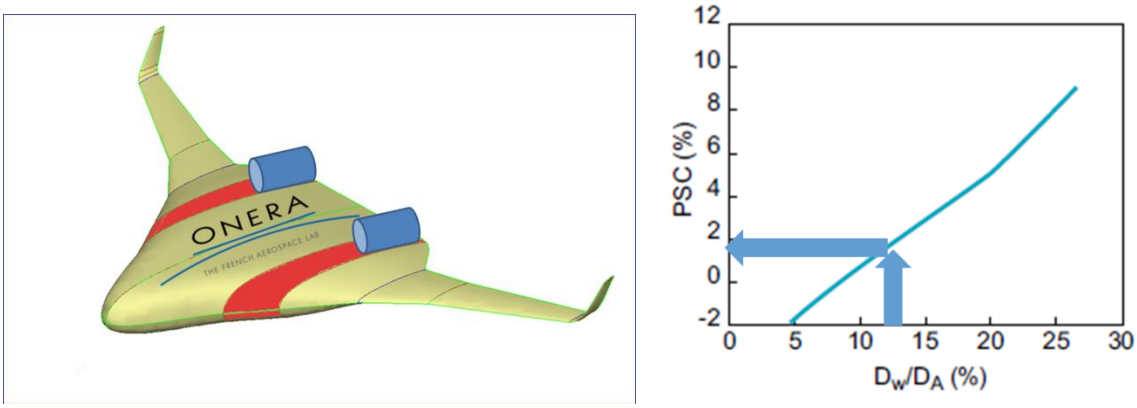

Figure 5: L0 BLI module - Left: "ingested surface" by the engines shown in red on a BWB concept Right: Original BLI chart from A. Plas MSc thesis [13].

Then using the Power Saving Coefficient chart from [13] provides a direct estimate of the BLI benefit.

The main drawback of that Level 0 method is that it does not account for important parameters driving the design of BLI engine integration such as fan characteristics or pressure gradients that modify the boundary layer profile. The purpose of Level 1 and Level 2 modules is to consider those effects.

3.2 Level 1 BLI process

In order to go deeper in the thermodynamic principles of BLI, a fan module is introduced to model the engine performance in the presence of a modified inflow. The computation of the average quantities enables to compute the right throttling for the engine and the necessary shaft power, and thus a more precise computation of the power saving coefficient. Main parameters of the model are the inlet capture stream tube and the engine characteristics (size and BPR/OPR/FPR). Regarding the modelling of boundary layer growth, a simple integral method is used in this L1 process. A power law provides then the boundary layer profiles, which are finally sent to a Power Balance method [14].

3.2.1 Boundary layer velocity profile using a power law

The first step of the process consists in growing a boundary layer, assuming a linear growth on a flat plate. The growth coefficient is 1cm/m, which is suitable for Reynolds numbers encountered on airliners and bizjets. As the Level 0 module, the Level 1 process neglects the pressure gradients that modify the boundary layer properties. The boundary layer velocity profile provides the input for the Power Balance postprocessing.

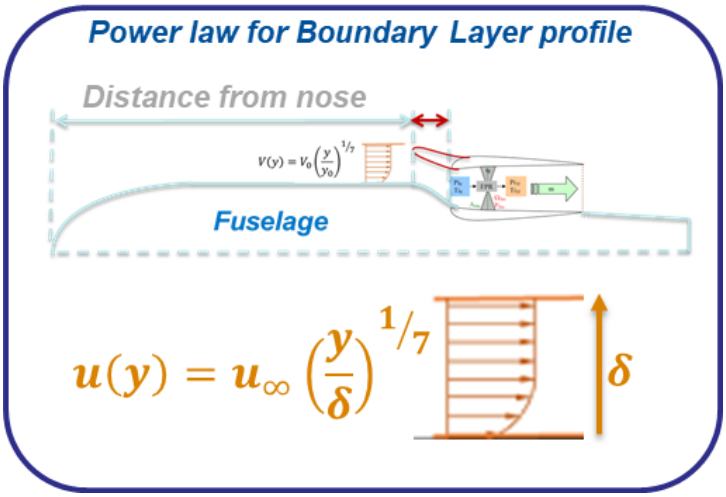

Figure 6: L1 BLI module - Schematic view of the power law used to model the boundary layer profile in front of the engine.

3.2.2 Power Balance method

The Power balance used in the process relies on the theory of Drela, [14], and especially the application by Hall [20]. The basics rely on the evaluation of the propulsive power P_k requested to propel the aircraft. Equation (2) is a simplified version of P_k, in which the propulsive power must compensate the aircraft drag (blue term), minus the power of the deficit of momentum ingested by the engines (green part in (2), which is always negative). That term is null in a non BLI case, because $u=u_\infty$. The last term in red corresponds to the excess of jet momentum behind the engines. In a BLI configuration, the engine ingests air at a lower velocity compared to a non-BLI configuration. Therefore, the exhaust velocity is slower in a BLI case (for a same mass flow rate and thrust setting), which makes the last term smaller in BLI. Even considering a similar aircraft drag power, the BLI configuration will require less power than the non-BLI one.

$$P_k = \Phi_{wake} + \Phi_{jet} + \cdots$$

$$P_k \approx \underbrace{\Phi_{wake}(noBLI)}_{\approx\ drag\ power} \underbrace{- \iint_{S_{inlet}} \frac{1}{2}(u_\infty - u)^2 \rho u.\, dS}_{<0} + \underbrace{\dot{m} u_\infty (u_{jet} - u_\infty)}_{Smaller\ with\ BLI} \quad (2)$$

Using the boundary layer profile in the BLI case, it is possible to compute the BLI savings coming from the three parts of equation (2). The following validation cases illustrate that possibility.

3.2.3 Low-speed validation: RAPRO2 test case

The first validation case is a wake ingestion experiment, which was performed at Onera, both with CFD and wind tunnel tests. This is an incompressible low-speed case (M=0.2), which is detailed in [6]. The main conclusion is a Power Saving Coefficient of 20% when the engine ingests all the wake of the blunt body, the engine diameter being the size of that wake (Figure 7).

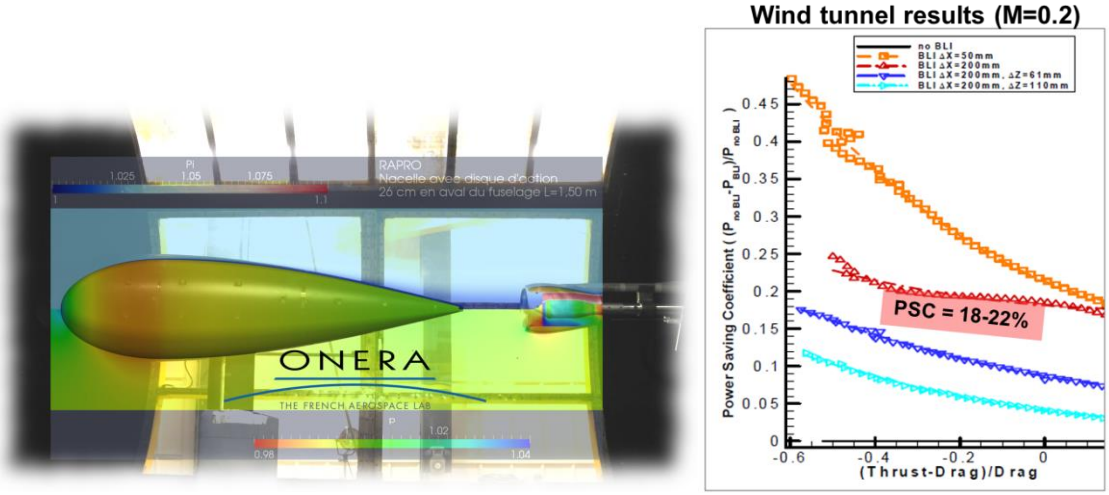

Figure 7: RAPRO2 experiment, showing an approximate 20% Power Saving Coefficient [6]

The Level 1 process integrated in MYSTIC provides results in line with the wind tunnel test results. The overall PSC=18.7% is close to the measurement (see Table 1). Furthermore, the process gives the contribution of the physics behind: 70% of the power saving comes from the ingestion of the wake, and 30% from the jet velocity reduction. Those figures are consistent with the experiment: the wake is thick, because the fore body has a large relative thickness ratio of 25% (max diameter / body length), so the $(u_\infty - u)^2$ in equation (2) is large. On the contrary, the jet velocity reduction is small, because the engine used for the test has a low Fan Pressure Ratio (FPR~1.05). That engine is an Electric Duct Engine from air models, sufficient for low speed tests. However, the lower the FPR, the slower the exhaust jet. Consequently, the gain in jet velocity between non-BLI and BLI is moderate, and the jet velocity reduction contributes only to 30% of the total PSC. The next validation case will show that the ranking can be different for engine with larger FPR.

Table 1: Validation results for Level 1 model

	RAPRO2	Transonic fuselage Rx=0	Transonic fuselage Rx=-0.0100
Wake saving (% of total)	0.12 kW (70%)	0.18 MW (30%)	0.18 MW (53%)
Jet saving(% of total)	0.05 kW (30%)	0.42 MW (70%)	0.16 MW (47%)
Total saving	0.17 kW	0.60 MW	0.34 MW
PSC L1	18.7% (20% in WTT)	21.6% (21% from CFD)	13.6% (13% from CFD)
PSC L0	~20%	~20%	

3.2.4 High-speed validation: generic transonic test case

The second validation case is purely numerical, and runs at Mach=0.82 (Figure 8). A generic axisymmetric fuselage generates a wake, which is ingested by an engine with a FPR~1.4 (so much larger than for the RAPRO2 experiment).

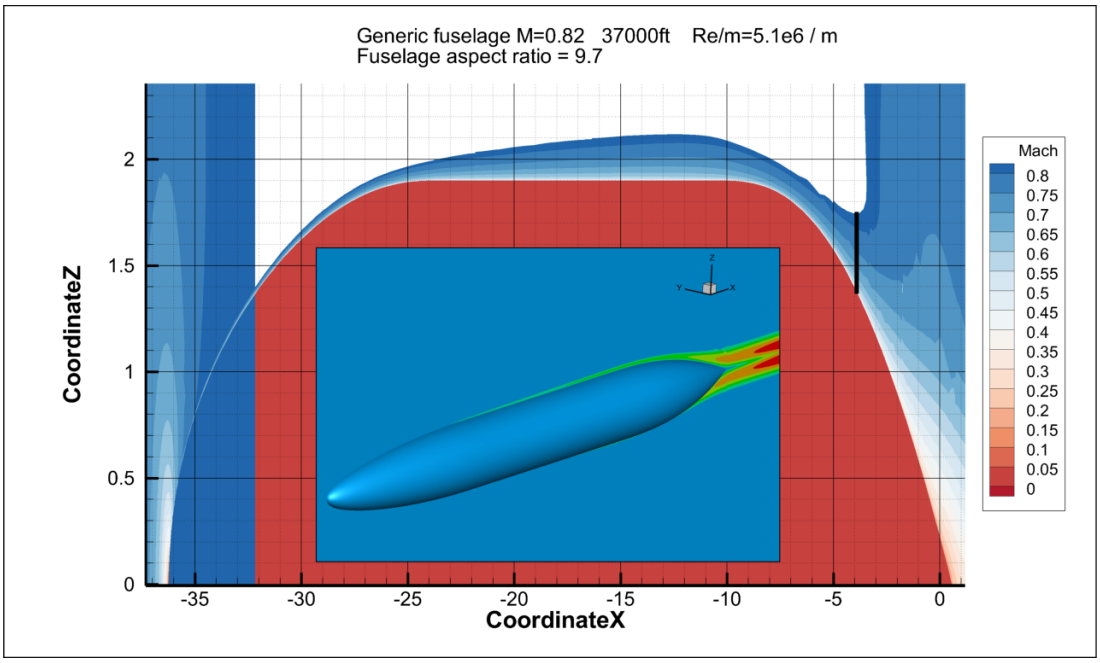

Figure 8: Generic fuselage shape (center), and Mach number in Y=0 plane, illustrating the boundary layer thickness. The engine virtual position is the black line at X=-4m.

The engine can be placed behind the fuselage (wake ingestion), or plugged on the fuselage (true BLI case), as illustrated in Figure 9. The engine contains a secondary flow only, and a body force model simulates the compression stage (fan and outlet guide vanes). The effect of the body force model adapts to the incoming flow: in Figure 9 top, the engine is producing a total pressure jump around FPR~1.4 when running isolated, whereas the pressure jump is only FPR~1.2 when ingesting the wake of the fuselage. That visible effect illustrates

the main effect of BLI, where the engine provides less energy to the flow for the same amount of thrust. Consequently, the exhaust flow velocity diminishes too.

The last 2 columns of Table 1 present the CFD results for two thrust settings. Rx=0 means that the overall resultant is null, i.e. the fuselage drag is perfectly compensated by the engine thrust. Rx=-0.01 stands for an excess of thrust of the engine, which corresponds to the missing drag that would come from virtual wings and tails.

The Level 1 module of MYSTIC is in good agreement with the CFD data (Table 1). At Rx=0, the PSC=21.6% is close to the 21% from CFD. In that case, 70% of the saving comes from the reduction of jet velocity. At Rx=-0.01, the PSC=13.6% fits also with CFD results, but the jet velocity reduction is smaller, so contributes less to the PSC (47% only).

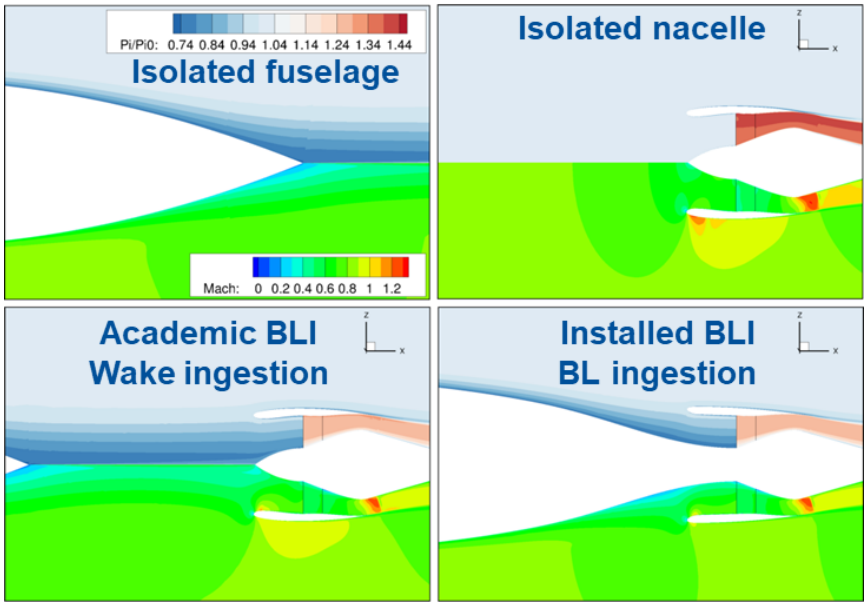

Figure 9: Possible configurations for the generic transonic fuselage (from [12]).

As a conclusion, the Level 1 method is able to capture trends and even absolute values for that generic test case. However, that method does not account for the pressure gradients that affect the boundary layer growth. That is the purpose of the Level 2 module.

3.3 Level 2 BLI process

The shape on which a boundary layer grows is not flat. It generates pressure gradients that influence the boundary layer shape. If that effect may be neglected on simple shapes, it is not accurate enough for a tube and wing configuration, for which the wing pressure field interacts with the boundary layer on the fuselage. It is even worse for a Blended Wing Body (BWB) configuration, the fuselage shape being a lifting airfoil with strong pressure gradients.

The purpose of the Level 2 process is to account for those effects, at OAD level, so with fast response tools (a few minutes per configuration). MYSTIC framework already has a fast CFD tool named CANOE (see §2.2), but that process relies on inviscid Euler computations, with no boundary layer. Switching to RANS CFD remains too costly nowadays (time of response within tens of minutes or few hours). Consequently, the following solution was

retained: a weak coupled boundary layer code. Figure 10 sketches the principle. From an Euler CFD results (skin pressure), the module extracts a pressure distribution along a line coming from the nose of the configuration up to the engine centerline. Then, using a simple integral method [21], a boundary layer grows downstream, taking into account the pressure gradient effects. At that stage, only the boundary layer coefficients are available, such as displacement thickness or momentum thickness. In order to feed the Power Balance module, it is necessary to have the boundary layer velocity profile. That step is performed by using a law of the wall close to the skin, and laws of the wake farther from the skin. Once available, the boundary profile is sent to the Power Balance module, but also to a Parallel Compressor Module (PCM) that provides an estimate of the fan losses when working in a distorted flow.

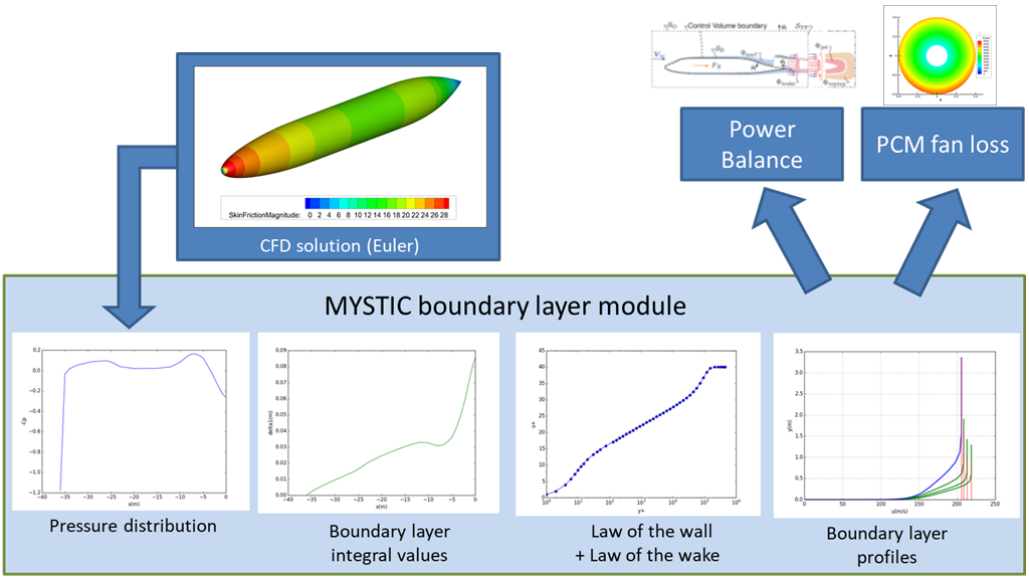

Figure 10: Level 2 BLI module - Schematic view.

3.3.1 Integral Boundary Layer method step (IBL)

Starting from CFD result (any pressure or velocity distribution, which may come from Euler or even panel method codes), a pressure distribution along a geometrical line is extracted and converted into a velocity distribution. The Integral Boundary Layer method (IBL, from [21] or [22]) requires the velocity derivative. As the later comes from a discretized mesh, a Savitzky-Golay filter smooths the signal. Then, using a step integration (from [21]), the module provides the boundary layer parameters.

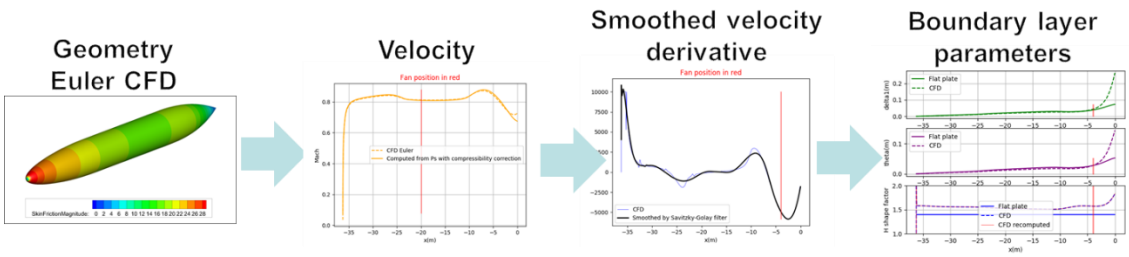

Figure 11: Level 2 BLI module - Integral Boundary Layer method step.

3.3.2 Velocity profile reconstruction using law of the wall and law of the wake.

The boundary layer velocity profile takes those coefficients as an input. Close to the wall (inner boundary layer, up to *y+=30*), a wall law is used. Beyond (outer boundary layer), two laws of the wake are implemented, from Coles [23] and Mellor & Gibson [24] (Figure 12).

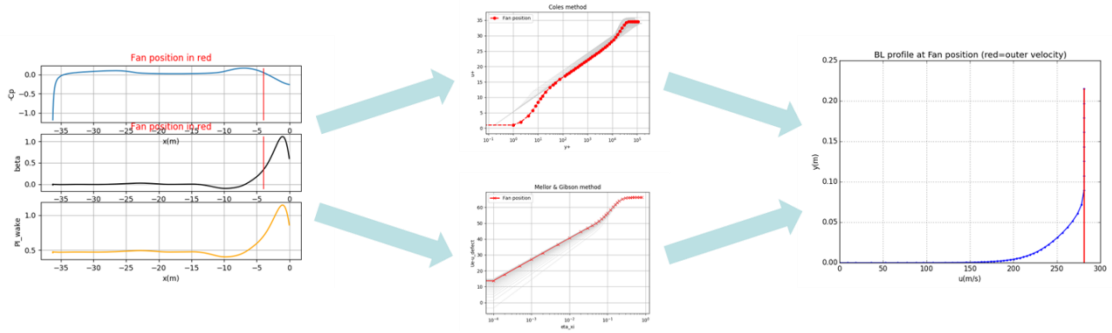

Figure 12: Level 2 BLI module - Generating the velocity profile.

Finally, the Power Balance module estimates the PSC with that boundary layer profile.

3.3.3 Parallel Compressor Module (PCM)

The Parallel Compressor Module is coded from [26]. Figure 13 illustrates the incoming boundary layer profiles (one for each 5 flight points), that are interpolated into 5 fan maps on a fictitious fan plane. The PCM module computes the local power consumption with those maps. Note that the power consumption is larger where the velocity is slower (so close to the fuselage wall), as expected. That explains part of the fan efficiency loss when working in a distorted flow (the real physics is more complex, but that simplification is enough at OAD level).

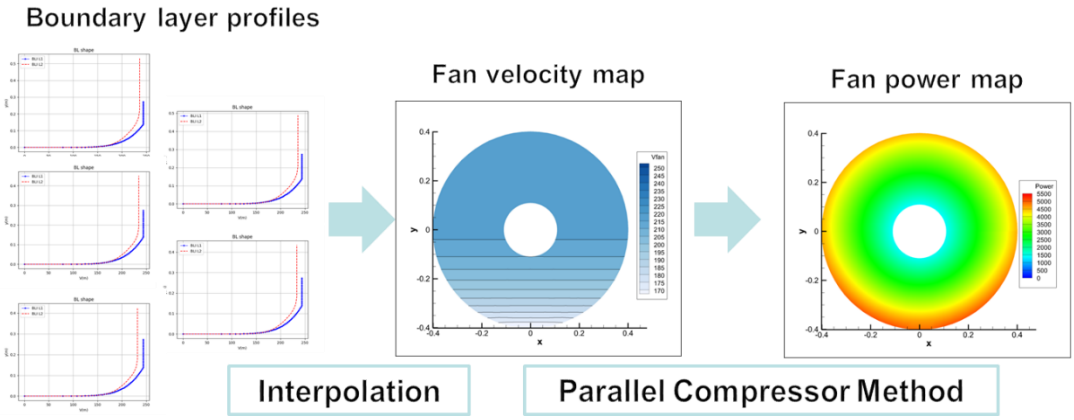

Figure 13: Level 2 BLI module - Parallel Compressor Method (PCM).

3.3.4 Validation on NASA flat plate

NASA 2D Zero Pressure Gradient Flat Plate (conditions corresponding to M=0.2, Re/m=5.10^6 m^{-1}) is used as a validation case [25]. Figure 14 presents the plots both with

u+=f(y+), but also *u=f(y)*. What matters mostly for BLI is the velocity loss within the boundary layer, but most of it relies in the outer part. The discrepancy on the inner part (Figure 14, left) has no impact on the BLI gain computation. That is why the Power law already provides a good estimate for the Level 1 module. Note that on the flat plate, all methods show very little discrepancy in the outer layer.

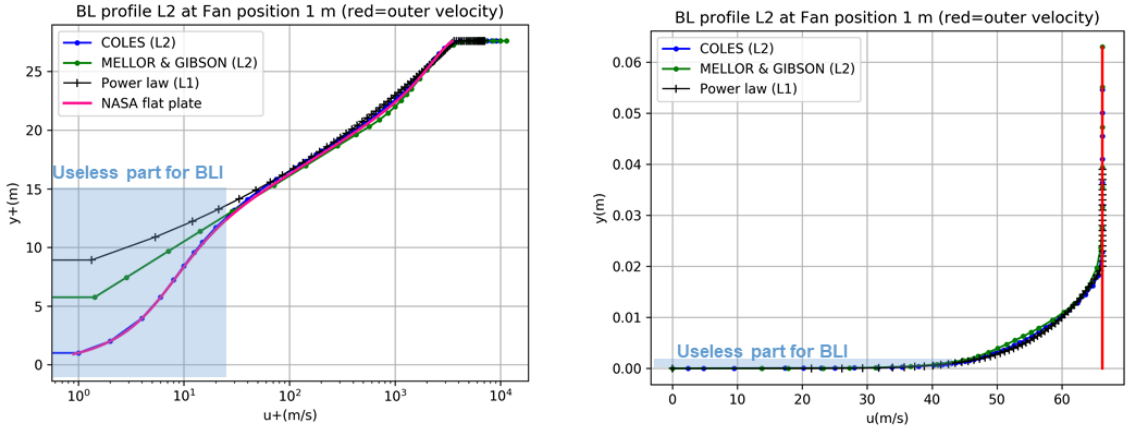

Figure 14: Level 2 BLI module - Comparing the reconstruction methods.

3.3.5 High-speed validation: generic transonic test case

The same case as in §3.2.4 is used for high-speed validation with pressure gradients, especially on the rear fuselage. A viscous RANS computation provides the targeted boundary layer velocity profile.

First, close to the fuselage nose (Figure 15), the boundary layer emerges from the long negative pressure gradient on the nose. That gradient tends to thin the boundary layer, compared to a flat plate. Indeed, the Power law is less accurate on that part, compared to Coles or Mellor & Gibson. Furthermore Mellor & Gibson is closer to CFD data.

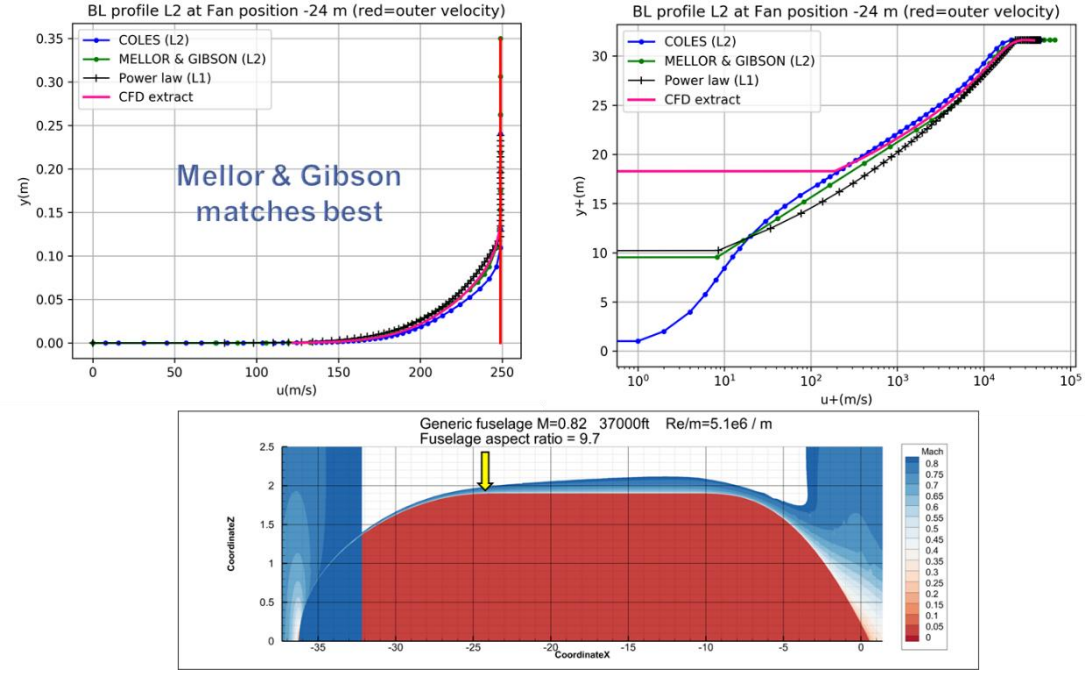

Figure 15: Generic transonic fuselage - Boundary layer close to the nose.

Travelling downstream (Figure 16), on the flat part of the fuselage, conclusions are similar. The Power law underestimates the velocity loss, and both law of the wake methods compared well with CFD. Close to the end of the cylindrical part (Figure 17), The Coles method is more accurate.

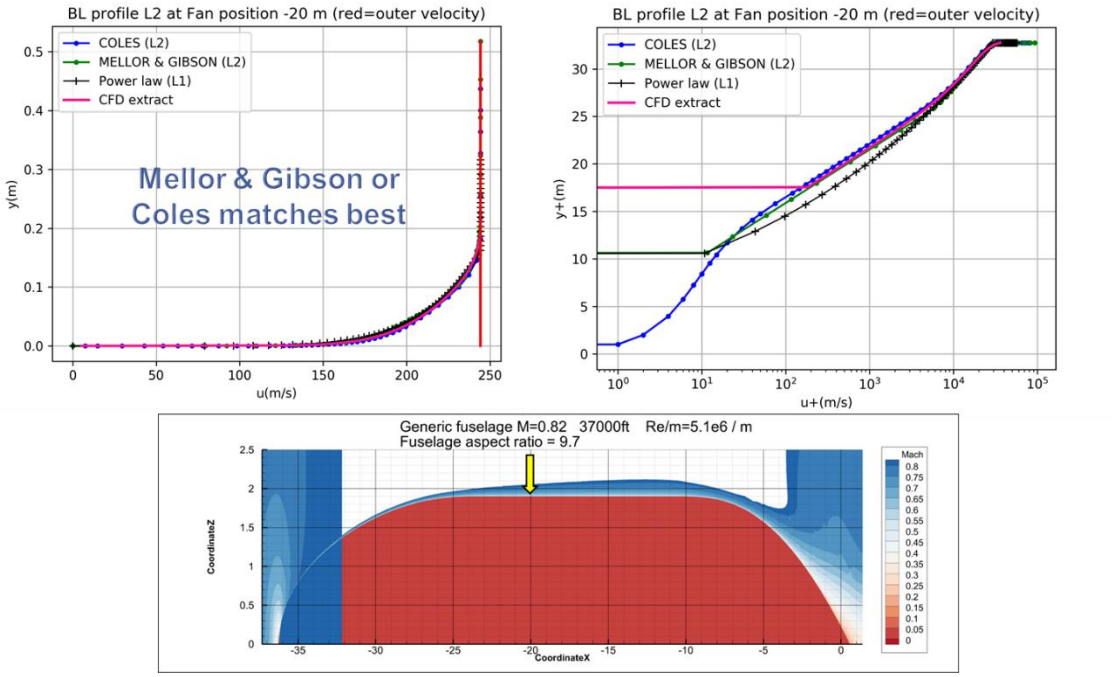

Figure 16: Generic transonic fuselage - Boundary layer on the flat part.

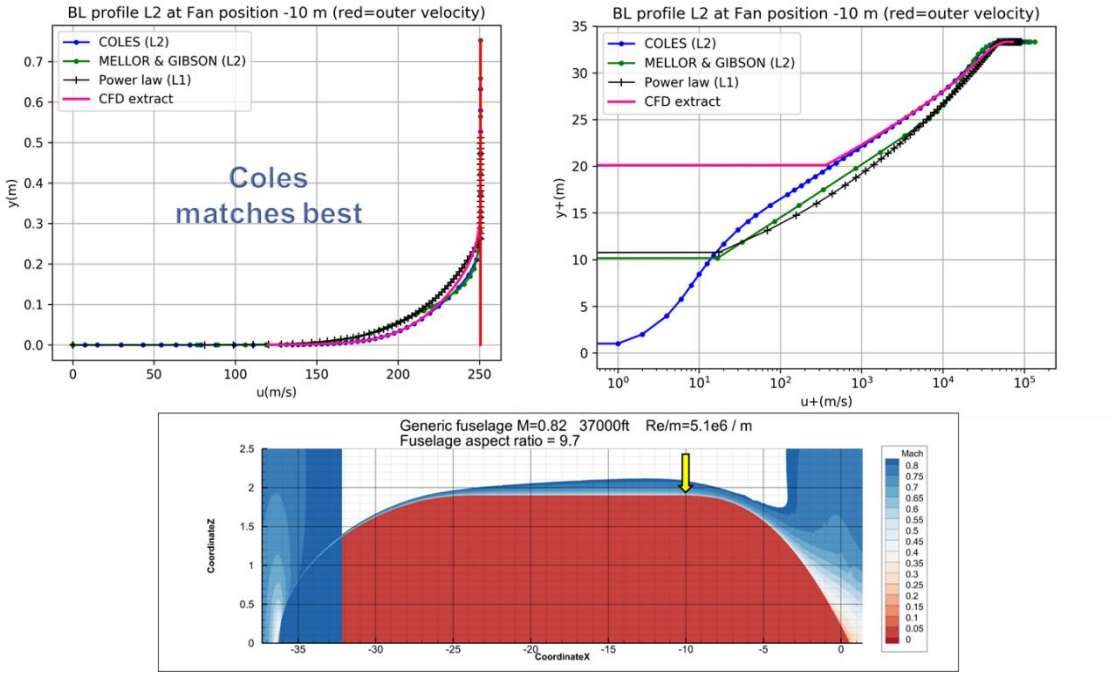

Figure 17: Generic transonic fuselage - Boundary layer end of cylindrical part.

Finally, in the recompression part with adverse pressure gradients (Figure 18), the Coles method is once again more in line with CFD results.

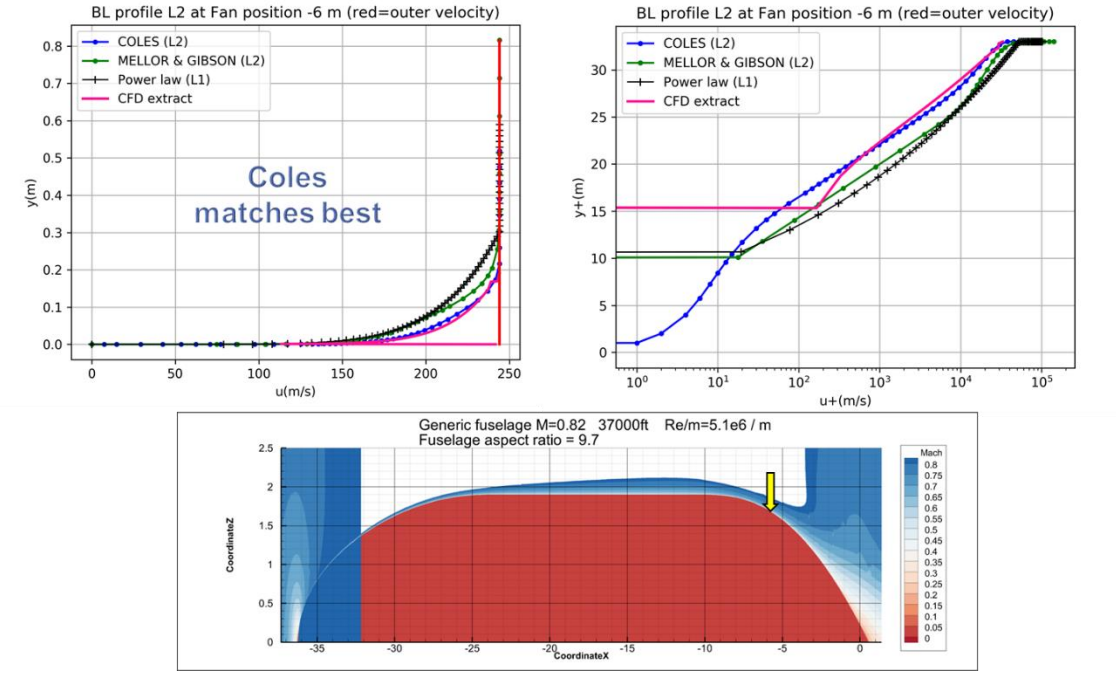

Figure 18: Generic transonic fuselage - Boundary layer end of recompression part.

As a conclusion, the Coles method is the preferred one for its reliability with respect to positive or negative pressure gradients. Note that the accuracy required for an OAD tool is not

the same as for a cruise drag estimation, so the Level 2 method is considered accurate enough for an OAD purpose.

4 APPLICATION: GENERIC WING BODY WITH 100% FUSELAGE BLI

4.1.1 Description of the test-case

One last case is a conceptual design named Common Inlet. The aircraft is representative of a business jet size and accommodates a twin engine (BPR=4.5), rear fuselage installation, for which each engine has a semi-circular intake that ingests half of the fuselage boundary layer (Figure 19). The concept is a challenge in terms of engine integration, but the purpose here is to estimate the potential benefit of such a BLI configuration.

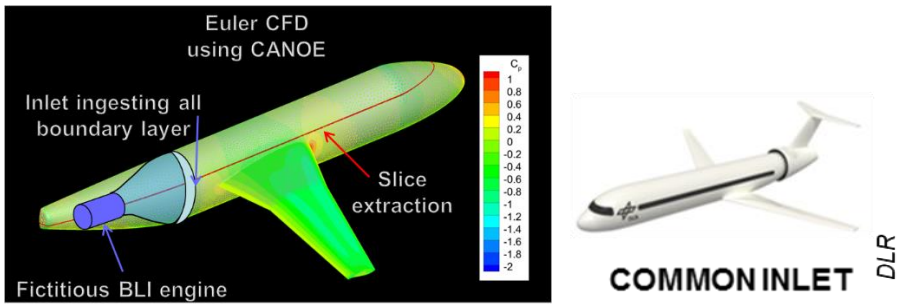

Figure 19: Common Inlet concept (right from DLR [10]).

The concept is modeled within MYSTIC as a simple tube and wing geometry. CANOE performs an Euler CFD computation on 5 flight points (various lift coefficients around cruise point), corresponding to Mach=0.75, 41000 ft. The unstructured mesh is generated automatically (2.6 million elements), each computation lasting 3 minutes on 128 CPU cores (Onera HPC). The slice extraction provides the pressure distribution, sent to the Level 2 module.

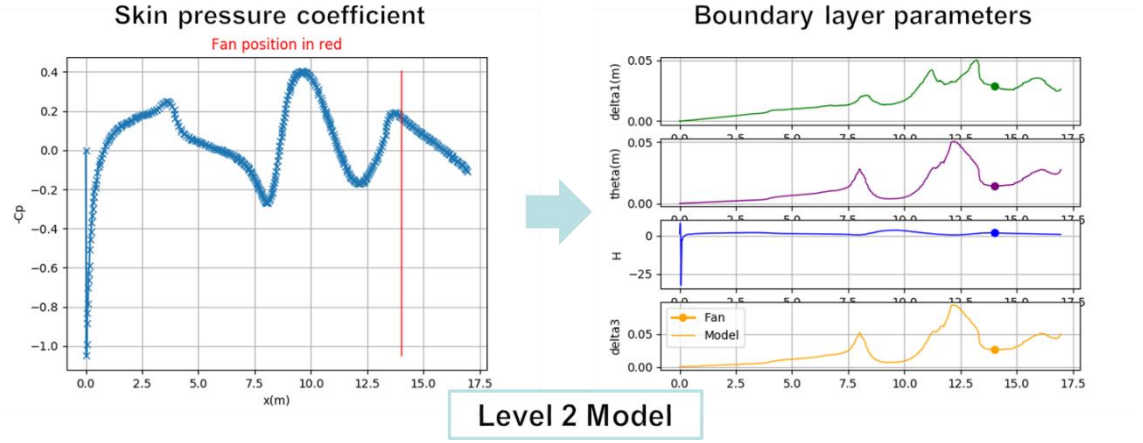

Figure 20: Common Inlet concept - Integral Boundary Layer method.

Figure 20 highlights the strong pressure gradients that the boundary layer encounters, especially the wing pressure effect between 7.5m<x<12.5m, and the resulting impact on boundary layer coefficients. The red line and the dots indicate the position of the air intake.

The reconstructed velocity profiles are sent to the Power Balance module, and also to the Parallel Compressor Module.

4.1.2 Results for the Common Inlet concept

Figure 21 summarizes the Level 1 and Level 2 results for the Common Inlet concept. Those results are obtained without any resizing loop in the MYSTIC process, especially the engines are not resized. Theoretically, in order to get the full benefits of BLI, it is preferable to compare engine configurations with similar mass flow rates ([20]), and adapted FPR such as the exhaust velocity is close to the upstream velocity in the BLI case. That allows maximizing the jet saving part in the Power Balance equation (2). Such a resizing loop was performed in [10] at L1 level, but was not performed on that Level 2 applicative case.

First, note that Level 1 results do not depend on the lift coefficient. As the Level 1 has no mean to create a dependency between the lift coefficient and the boundary layer, the BLI gain is assumed constant all along the flight. When using MYSTIC along a complete flight path, that assumption is optimistic. The same rule applies to the fan loss which is null or arbitrarily constant.

On the contrary, the Level 2 module provides a PSC that depends on the flight point. It is possible to run the module for take-off, climb or other flight conditions, thus providing a more accurate accounting of the BLI benefits all along the aircraft trajectory.

The Level 2 PSC~3%, (without resizing loop) is downgraded by the fan loss that can reach 1.5% for high distortion levels. Thanks to those data, MYSTIC OAD process can interpolate the real flight condition and account for the BLI effect, both on the lift-to-drag ratio and the Specific Fuel Consumption.

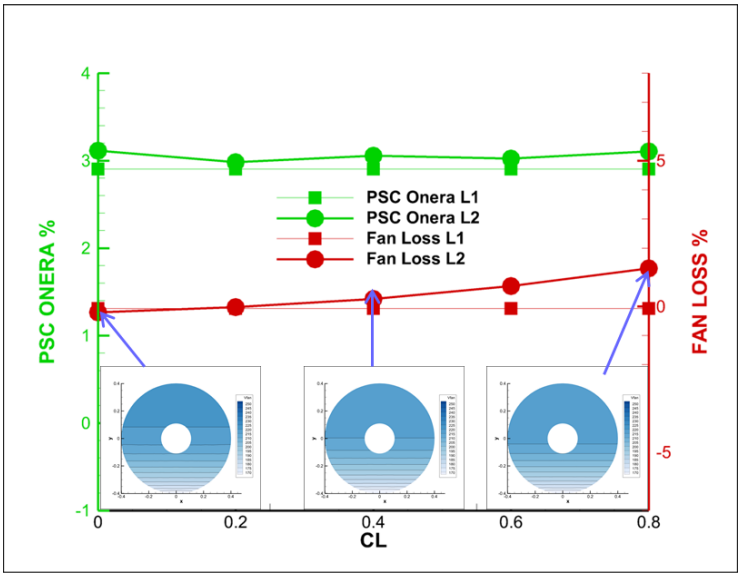

Figure 21: Common Inlet concept - PSC and fan losses.

5 CONCLUSION

The multi-fidelity MYSTIC OAD process has been enriched with two BLI modules of different levels of fidelity. At each step, a validation process is performed with existing experimental or numerical datasets. The accuracy reached with both Level 1 and Level 2 modules is assumed to be sufficient for an OAD tool.

These modules were applied to the common inlet concept which aims at ingesting 100% of the fuselage boundary layer. The results demonstrate the potential gain on the Power Saving Coefficient (up to 3% obtained with the L2 BLI module without resizing loop) but with non-negligible fan losses (up to 1.5%).

Next steps consist in further validation with upcoming experiments and numerical applications, and application to a various set of novel aircraft configurations, such as Blended Wing Body or distributed propulsion on the rear fuselage. Parametric explorations such as engine positioning and size or inlet shape will be enabled by this enhanced OAD process.

6 ACKNOWLEDGMENTS

The project leading to this application has received funding from the Clean Sky 2 Joint Undertaking under the European Union's Horizon 2020 research and innovation program under grant agreement N°CS2-AIR-GAM-2020-2021-01. The authors would like to thank the project partners from DLR (Michael Iwanizki, Thomas Zill, B. Froehler), Dassault Aviation (Jean Le Gall, Michel Ravachol) and Airbus Commercial Aircraft (Lars Joergensen) for their interest in this topic and their guidance.

REFERENCES

[1] Smith L. H. Jr., "*Wake Ingestion Propulsion Benefit*", Journal of Propulsion and Power, Vol. 9, No. 1, 1993, pp. 74–82.

[2] J. I. Hileman, Z. S. Spakovszky, M. Drela, "*Airframe Design for "Silent Aircraft"* ", AIAA 2007-453, 2007

[3] David J. Arend, Gregory Tillman, Walter F. O'Brien, "*Generation After Next Propulsor Research: Robust Design for Embedded Engine Systems*", AIAA 2012-4041, 2012

[4] Uranga A., et al. *Preliminary Experimental Assessment of the Boundary Layer Ingestion Benefit for the D8 Aircraft*, 52nd Aerospace Sciences Meeting, January 13-17, 2014, National Harbor, Maryland

[5] Plas, A., Crichton, D., Sargeant, M., Hynes, T., Greitzer, E., Hall, C. and Madani, V. 2007. *Performance of a Boundary Layer Ingesting (BLI) Propulsion System*. 45th AIAA Aerospace Sciences Meeting and Exhibit (Reno, Nevada, Jan. 2007). ISBN 9781624100123. DOI 10.2514/6.2007-450.

[6] Atinault O., Carrier G., Grenon R., Verbeke C. and Viscat P., "*Numerical and Experimental Aerodynamic Investigations of Boundary Layer Ingestion for Improving Propulsion Efficiency of Future Air Transport*", 31st AIAA Applied Aerodynamics Conference, June 24-27, 2013, San Diego, CA.

[7] Isikveren, A.T., Seitz, A., Bijewitz, J., Mirzoyan, A., Isyanov, A., Grenon, R., Atinault, O., Godard, J.-L. and Stückl, S. 2015. *Distributed propulsion and ultra-high by-pass rotor study at aircraft level*. The Aeronautical Journal. 119, 1221 (Nov. 2015), 1327–1376. ISSN 0001-9240, 2059-6464. DOI 10.1017/S0001924000011295.

[8] Blumenthal, B., Elmiligui, A.A., Geiselhart, K., Campbell, R.L., Maughmer, M.D. and Schmitz, S. 2016. *Computational Investigation of a Boundary Layer Ingestion Propulsion System for the Common Research Model*. 46th AIAA Fluid Dynamics Conference (Washington, D.C., Jun. 2016). ISBN 9781624104367. DOI 10.2514/6.2016-3812.

[9] Welstead, J. and Felder, J.L. 2016. *Conceptual Design of a Single-Aisle Turboelectric Commercial Transport with Fuselage Boundary Layer Ingestion*. 54th AIAA Aerospace Sciences Meeting (San Diego, California, Jan. 2016). ISBN 9781624103933. DOI 10.2514/6.2016-1027

[10] M. Méheut and al. "*Conceptual Design Studies of Boundary Layer Engine Integration Concepts*", Aerospace Europe Conference 2020, 25-28 February 2020, Bordeaux, France.

[11] Wiart, L., Atinault, O., Boniface, J.-C. and Barrier, R. 2016. *Aeropropulsive performance analysis of the NOVA configurations*. 30th Congress of the International Council of the Aeronautical Sciences (Daejeon, South Korea, Sep. 2016).

[12] Wiart, L. and Negulescu, C. 2018. *Exploration of the Airbus "NAUTILIUS" Engine Integration Concept*. 31st Congress of the International Council for Aeronautical Sciences (Belo Horizonte, Brazil, Sep. 2018).

[13] Plas A., *Performance of Boundary Layer Ingesting Propulsion System*, MSc Thesis, Massachusetts Institute of Technology, 2006

[14] Drela, M., "*Power Balance in Aerodynamic Flows*", AIAA Journal, Vol. 47, No. 7 (2009), pp. 1761-1771.

[15] Liu, Chengyuan, Daniel Ihiabe, Panagiotis Laskaridis, Riti Singh, "*A Preliminary Method to Estimate Impacts of Inlet Flow Distortion on Boundary Layer Ingesting Propulsion System Design Point Performance*", JAERO1774R1, 2014
[16] S. Defoort, M. Méheut , B. Paluch , R. Liaboeuf , R. Murray , D.-C. Mincu , J.M. David, *Conceptual design of disruptive aircraft configurations based on High-Fidelity OAD process*", AIAA Aviation Forum, Atlanta, 2018.
[17] T. D. Economon, F. Palacios, S. R. Copeland, T. W. Lukaczyk, and J. J. Alonso, *SU2: An open- source suite for multiphysics simulation and design*, AIAA Journal, 54(3):828-846, 2016. doi: 10.2514/1.J053813.
[18] J. van der Vooren J., Destarac D., *Drag/Thrust Analysis of a Jet-propelled Transonic Transport Aircraft; Definition of Physical Drag Components*, Aerospace Science & Technology 8 (2004), pp. 545-556, September 2004.
[19] Chaput, A., Rizo-Patron, S., *Vehicle Sketch Pad Structural Analysis Module Enhancements for Wing Design*, 50th AIAA Aerospace Sciences Meeting, Nashville, TN, 2012, AIAA-2012-546
[20] Hall David K., *Boundary Layer Ingestion Propulsion Benefit for Transport Aircraft*, Journal Of Propulsion And Power Vol. 33, No. 5, September–October 2017
[21] Cousteix, J., *Turbulence et couche limite*, Cepadues, 1989
[22] H. Schlichting, K. Gersten, *Boundary Layer Theory*, Springer, 2000
[23] Coles, D E, *The law of the wake in the turbulent boundary layer*. Journal of Fluid Mechanics, Vol 1, p 191, 1956.
[24] Mellor and Gibson, *Equilibrium turbulent boundary layers*, J. Fluid Mech. (1966), vol. 44, part 2, pp. 225-253
[25] https://turbmodels.larc.nasa.gov/flatplate.html
[26] Budziszewski N, Friedrichs J. *Modelling of A Boundary Layer Ingesting Propulsor*. Energies. 2018; 11(4):708. https://doi.org/10.3390/en11040708
[27] Hang Si. 2015. *TetGen, a Delaunay-Based Quality Tetrahedral Mesh Generator*. ACM Trans. on Mathematical Software. **41** (2), Article 11 (February 2015), 36 pages. DOI=10.1145/2629697 http://doi.acm.org/10.1145/2629697
[28] https://ceras.ilr.rwth-aachen.de/tiki/tiki-index.php?page=CSR-01
[29] https://github.com/fast-aircraft-design/FAST-OAD